Journal of Thermal Analysis and Calorimetry (2024) 149:4691–4708
https://doi.org/10.1007/s10973-024-13028-4

# Investigation on in-cylinder and in-intercooler thermodynamic properties of miniature multi-stage reciprocating compressor with insufficient inter-stage volumes

**Yipan Deng[1] · Xin Jiang[1] · Wang Chuanmin[1] · Longfei Bai[1] · Yinshui Liu[1] · Kuihua Hu[2]**

Received: 30 March 2023 / Accepted: 26 February 2024 / Published online: 12 May 2024


**Abstract**
Miniature multi-stage reciprocating compressor is the core component in the on-board continuous high-pressure gas supply system. Intercoolers play an important role in determining the thermodynamic performance of multi-stage reciprocating compressor. However, adequate inter-stage volume cannot be provided to miniature multi-stage reciprocating compressor due to the restriction of compacted dimension. Understanding the thermodynamic performance with insufficient inter-stage volume is the key issue for design and application of miniature multi-stage reciprocating compressor. However, the previous work focused on the thermodynamic process in single-stage cylinder, the proposed model cannot predict the real-time thermodynamic process in intercoolers. In this paper, stage-in-series thermodynamic model has been established by connecting the multi-stage cylinders through the intercoolers and the internal transient heat transfer was emphasized. The in-cylinder and in-intercooler thermodynamic properties have been numerically analyzed under insufficient inter-stage volumes. Experimental investigation on compressor performance has been carried out by varying the intercooler channel diameter. The results show that insufficient inter-stage volumes bring about the abnormal movement of suction and discharge valves. Pressure peak in former-stage cylinders increases when the inter-stage volume decreases, which results in obvious increase in frictional loss and power consumption. This study provides significant references for design optimization of miniature multi-stage reciprocating compressor. Furthermore, the proposed methods can be applied to large-scale reciprocating compressor for improving efficiency and reducing power consumption.

**Keywords** Intercoolers · Thermodynamic property · Miniature multi-stage compressor · Insufficient inter-stage volume

**List of Symbols**

| | |
|---|---|
| $A$ | Area/m$^2$ |
| $m$ | Air mass/kg |
| $p$ | Gas pressure/Pa |
| $Q$ | Heat/J |
| $T$ | Temperature/K |
| $u$ | Internal energy/J kg$^{-1}$ |
| $h$ | Specific enthalpy/J kg$^{-1}$ |
| $W$ | Work/J |
| $V$ | Volume/m$^3$ |
| $M$ | Valve plate mass/kg |
| $s$ | Piston displacement/m |
| $s_{max}$ | Piston stroke/m |
| $r$ | Valve orifice radius/m |
| $l$ | Length of flow channel/m |
| $R_0$ | Cylinder distribution radius/m |
| $C_d$ | Orifice discharge coefficient |
| $C_r$ | Rebound coefficient |
| $k_s$ | Suction valve spring stiffness/N m$^{-1}$ |

✉ Yinshui Liu
liuwater@hust.edu.cn

[1] School of Mechanical Science and Engineering, Huazhong University of Science and Technology, No. 1037, Luoyu Road, Wuhan, China

[2] CAMA (Luoyang) Gas Supply Co., Ltd.,, Luoyang, China

$k_d$ Discharge valve spring stiffness/N $m^{-1}$
$z_{s0}$ Pre-compression length of suction valve spring/m
$z_{d0}$ Pre-compression length of discharge valve spring/m
Gr Grashof number
Pr Prandtl number

**Greek letters**

$\gamma$ Swash plate angle/°
$\omega$ Angular speed/rad $s^{-1}$
$\theta$ Degree/rad
$\rho$ Gas density/kg $m^{-3}$
$\varepsilon$ Compression ratio
$\delta$ Wall thickness/m
$\alpha$ Heat transfer coefficient/W $m^{-2}$ $K^{-1}$
$\lambda$ Thermal conductivity/W $m^{-1}$ $K^{-1}$
$\eta$ Dynamic viscosity/Pa s
$\tau$ Mean velocity of piston/m $s^{-1}$
$\psi$ Overall heat transfer coefficient/W $m^{-2}$ $K^{-1}$
$\vartheta$ Relative clearance volume rate

**Subscripts**

s Suction
d Discharge
cy In-cylinder
ic Intercooler
co Coolant
p Piston
e Inlet of intercooler
f Outlet of intercooler
w Wall surface

## Introduction

On-board continuous supply system of high-pressure clean gas has been widely applied to aircraft for missions of missile launching and infrared cooling, which can eliminate the need for gas canisters and refills, improve mission flexibility and forward deployment. Miniature multi-stage reciprocating compressor with compacted size and high output pressure is the crucial component in the on-board continuous gas supply system, and its thermodynamic properties have significant influence on the working performance of the system [1]. Intercoolers which can store and cool the inter-stage gas play an important role in determining the overall performance of multi-stage reciprocating compressor [2]. Traditional multi-stage reciprocating compressor holds large size and the internal volume of intercoolers usually is more than 10 times the stroke volume of the subsequent-stage cylinder, which means the sufficient inter-stage gas can be stored and cooled for subsequent-stage cylinder [3, 4]. Therefore, little attention was paid to the effects of intercooler volume and single-stage mathematical model was applied to analyze the thermodynamic properties of multi-stage compressor by changing the suction and discharge parameters [5, 6]. However, for miniature multi-stage reciprocating compressor, adequate intercooler volume cannot be provided due to the restriction of compacted dimension. Gas storage capacity and cooling capacity of intercoolers are greatly weakened, which can exert significant influence on the thermodynamic performance of the compressor.

Many previous research have been carried out to investigate the in-cylinder thermodynamic properties of reciprocating compressor based on single-stage mathematical model. Navarro et al. [7] developed a mathematical model for reciprocating compressor, and a statistical fitting methodology based on Monte Carlo techniques was designed to predict volumetric efficiencies with an error lower than 3% under a wide range of operating conditions. Yang et al. [8] presented a comprehensive simulation model including frictional power loss and piston leakage for a reciprocating compressor, mass flow rate, input power and efficiency which were predicted. Farzaneh-Gord et al. [9, 10] established the mathematical model of single-stage reciprocating compressor, and the effects of natural gas composition were evaluated by inducing special gas state equation. A differential model for reciprocating compressors was developed by Roskosch et al. [11] to calculate volumetric and isentropic efficiencies as a function of the inlet condition and the outlet pressure and the fluid. A novel generalized framework is presented by Bell et al. [12] to simulate the quasi-steady-state performance of a wide range of positive displacement compressors. Wang et al. [13] derived a thermodynamic model of reciprocating compressor from the experimental *p–V* diagram in the expansion and compression phases, and the internal mass transport process was analyzed. Apart from mathematical models, CFD method has been applied to investigate the complex flow inside the cylinders [14]. Zhao et al. [1, 15] used mesh mapping method combining with dynamic mesh technique to simulate the transient flow inside the reciprocating compressor. Wang et al. [13] also developed a three-dimensional fluid structure interaction (FSI) model to investigate delayed closure and oscillation of suction valve in reciprocating compressors. Wu et al. [16] simulated the motion of the valve on the piston inside a single acting compressor by the FSI method. To sum up, the existing research focused on the thermodynamic process inside the single-stage cylinder of reciprocating compressor. The effects of intercooler cannot be considered in the proposed methods and the overall thermodynamic properties of multi-stage reciprocating compressor cannot be predicted precisely.

This study investigates in-cylinder and in-intercooler thermodynamic properties of miniature multi-stage reciprocating compressor with insufficient inter-stage volumes.

Stage-in-series mathematical models have been established by connecting the multi-stage cylinders with intercoolers, and the transient heat transfer inside the intercoolers has been considered. The effects of intercooler channel diameter on the compressor performance have been investigated numerically and experimentally. This work provides significant references for design optimization of miniature multi-stage reciprocating compressor. Furthermore, the proposed numerical methods can be applied to large-scale reciprocating compressor for improving efficiency and reducing power consumption.

## Numerical modeling

### Schematic of miniature multi-stage reciprocating compressor

The working principle of the miniature multi-stage reciprocating compressor is presented in Fig. 1. Multi-stage pistons are mounted in the integrated cylinder block and driven by swash plate. Integrated suction valves, discharge valves and intercoolers are used to shorten the axial dimension. Gas inhaled from the inlet is compressed stage by stage to form high pressure, and the inter-stage gas is cooled by forced coolant flow.

Based on the schematic diagram, the motion equation of multi-stage pistons can be given as following[17].

$$s_i = R_0[1 - \cos(\omega t + \theta_{i0})]\tan\gamma \tag{1}$$

where $R_0$ is the distribution circle radius of the pistons, $\omega$ is the angular speed of motor, $\gamma$ is the swash plate angle, and $\theta_{i0}$ is the initial phase angle of $i$th piston.

Therefore, the volume inside the $i$th cylinder can be calculated as following.

$$V_{cyi} = \frac{\pi}{4}D_{pi}^2\left(s_i + s_{max}\vartheta_i\right) \tag{2}$$

where $D_{pi}$ is the $i$th piston diameter and $\vartheta_i$ is the relative clearance volume rate of the $i$th cylinder. The values of first piston, second piston, third piston and fourth piston are 44 mm, 22 mm, 10 mm and 6 mm, respectively.

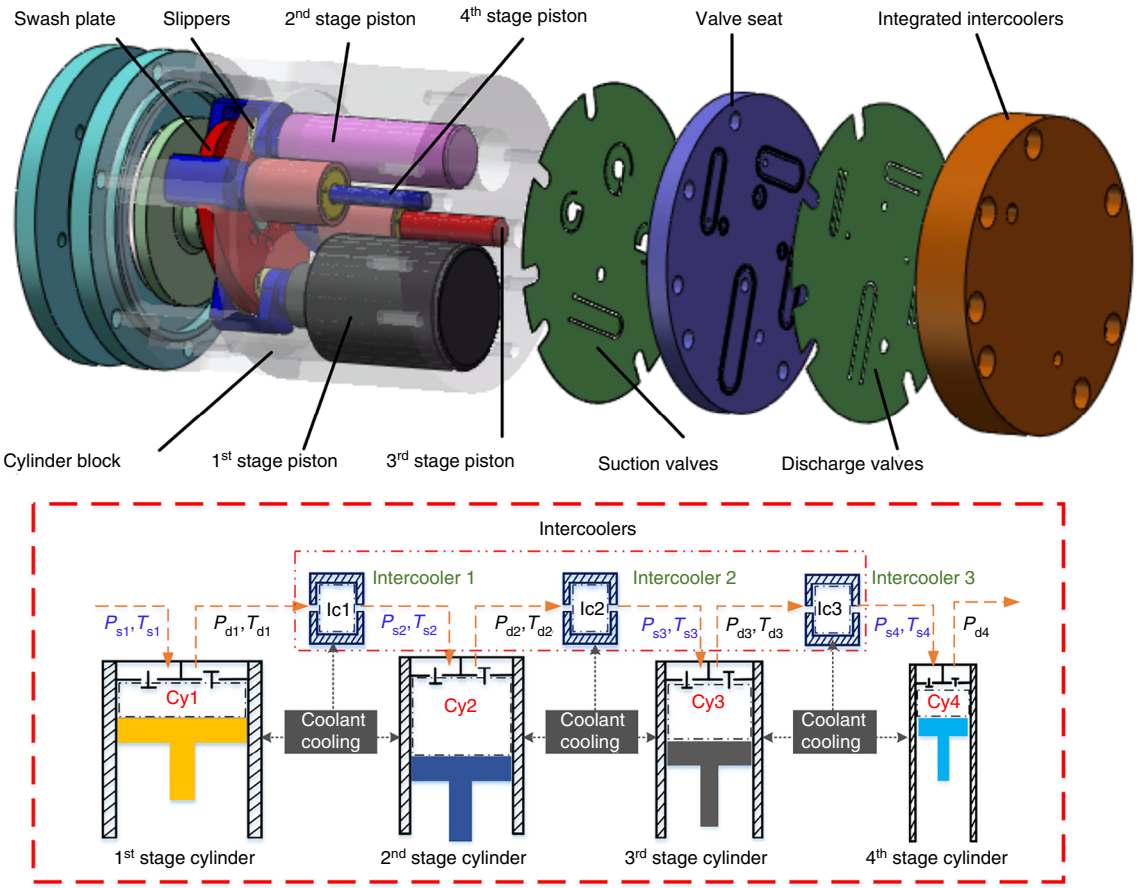


**Fig. 1** Schematic of miniature multi-stage reciprocating compressor

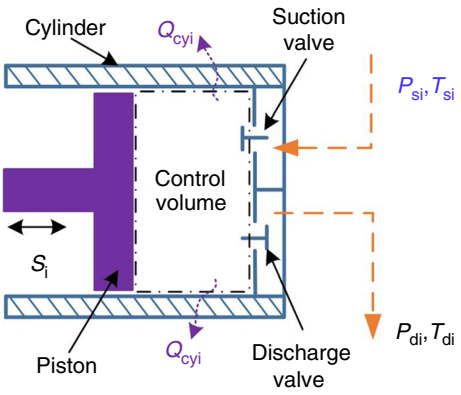


**Fig. 2** Schematic of thermodynamic process in cylinders

## Thermodynamic process in cylinders

The ideal gas state equation is used to establish the stage-in-series thermodynamic model of miniature multi-stage reciprocating compressor. Gas inside the control volume of cylinder is regarded as homogeneous, and the kinetic energy and potential energy are ignored [18]. Additionally, the gas leakage through the pistons is neglected due to PTFE rings with excellent sealing performance are used.

The schematic of thermodynamic process in multi-stage cylinders is presented in Fig. 2. The basic equations for the control volume can be listed as following.

1. Energy and mass model [19]

$$\frac{\mathrm{d}}{\mathrm{d}t}\left(m_{\mathrm{cvi}}u_{\mathrm{cvi}}\right)=\frac{\mathrm{d}Q_{\mathrm{cvi}}}{\mathrm{d}t}+h_{\mathrm{si}}\frac{\mathrm{d}m_{\mathrm{si}}}{\mathrm{d}t}-h_{\mathrm{di}}\frac{\mathrm{d}m_{\mathrm{di}}}{\mathrm{d}t}-\frac{\mathrm{d}W_{\mathrm{cvi}}}{\mathrm{d}t} \quad (3)$$

The work term $\frac{\mathrm{d}W_{\mathrm{cvi}}}{\mathrm{d}t}$ can be written as [19]

$$\frac{\mathrm{d}W_{\mathrm{cvi}}}{\mathrm{d}t}=p_{\mathrm{cvi}}\frac{\mathrm{d}V_{\mathrm{cvi}}}{\mathrm{d}t} \quad (4)$$

The item $\frac{\mathrm{d}}{\mathrm{d}t}\left(m_{\mathrm{cvi}}u_{\mathrm{cvi}}\right)$ can be further calculated as following.

$$\begin{aligned}\frac{\mathrm{d}}{\mathrm{d}t}\left(m_{\mathrm{cvi}}u_{\mathrm{cvi}}\right)=&u_{\mathrm{cvi}}\frac{\mathrm{d}\left(m_{\mathrm{cvi}}\right)}{\mathrm{d}t}+m_{\mathrm{cvi}}\frac{\mathrm{d}\left(u_{\mathrm{cvi}}\right)}{\mathrm{d}t}=m_{\mathrm{cvi}}\frac{\mathrm{d}h_{\mathrm{cvi}}}{\mathrm{d}t}\\&+h_{\mathrm{cvi}}\frac{\mathrm{d}m_{\mathrm{cvi}}}{\mathrm{d}t}-p_{\mathrm{cvi}}\frac{\mathrm{d}V_{\mathrm{cvi}}}{\mathrm{d}t}-V_{\mathrm{cvi}}\frac{\mathrm{d}p_{\mathrm{cvi}}}{\mathrm{d}t}\end{aligned} \quad (5)$$

Therefore, Eq. (3) can be finally expressed as following.

$$\frac{\mathrm{d}Q_{\mathrm{cvi}}}{\mathrm{d}t}+h_{\mathrm{si}}\frac{\mathrm{d}m_{\mathrm{si}}}{\mathrm{d}t}=h_{\mathrm{di}}\frac{\mathrm{d}m_{\mathrm{di}}}{\mathrm{d}t}+m_{\mathrm{cvi}}\frac{\mathrm{d}h_{\mathrm{cvi}}}{\mathrm{d}t}+h_{\mathrm{cvi}}\frac{\mathrm{d}m_{\mathrm{cvi}}}{\mathrm{d}t}-V_{\mathrm{cvi}}\frac{\mathrm{d}p_{\mathrm{cvi}}}{\mathrm{d}t} \quad (6)$$

Additionally, mass conversation equation can be written as following [18].

$$\frac{\mathrm{d}m_{\mathrm{cvi}}}{\mathrm{d}t}=\frac{\mathrm{d}m_{\mathrm{si}}}{\mathrm{d}t}-\frac{\mathrm{d}m_{\mathrm{di}}}{\mathrm{d}t} \quad (7)$$

2. Heat transfer model.

As for the heat transfer between in-cylinder gas and cylinder wall, the following equation can be used [20].

$$\frac{\mathrm{d}Q_{\mathrm{cvi}}}{\mathrm{d}t}=\alpha_{\mathrm{cyi}}A_{\mathrm{cyi}}\left(T_{\mathrm{cyi}}-T_{\mathrm{wi}}\right) \quad (8)$$

where $\alpha_{\mathrm{cyi}}$, $T_{\mathrm{cyi}}$ and $T_{\mathrm{wi}}$ are the heat transfer coefficient, in-cylinder gas temperature, and wall temperature, respectively. $A_{\mathrm{cyi}}$ represents in-cylinder surface area contacted with gas which varies with piston displacement.

The convective heat transfer coefficient $\alpha_{\mathrm{cyi}}$ can be calculated according to Woschni correlation as below [11, 21].

$$\alpha_{\mathrm{cy\,i}}=127.93D_{\mathrm{pi}}^{-0.2}p_{\mathrm{cyi}}^{0.8}T_{\mathrm{cyi}}^{-0.53}\left(\beta\tau_{\mathrm{pi}}\right)^{0.8} \quad (9)$$

where $\tau_{\mathrm{pi}}$ and $D_{\mathrm{pi}}$ are the mean velocity and diameter of the $i$th piston, respectively. The value of parameter $\beta$ is 6.18 when the suction valve or discharge valve is open and 2.28 vice versa.

The wall temperature $T_{\mathrm{wi}}$ can be defined as following [22].

$$T_{\mathrm{wi}}=211+0.3T_{\mathrm{si}}+0.162\omega+8\left(\varepsilon_{\mathrm{i}}-1\right) \quad (10)$$

where $\varepsilon_{\mathrm{i}}$ is the real-time compression ratio.

(3) Valve motion.

Considering the possible back flow, the mass flow through the suction valves and discharge valves is given in Eqs. (11) and (12), respectively [23].

$$\frac{\mathrm{d}m_{\mathrm{si}}}{\mathrm{d}t}=\begin{cases}\frac{C_{\mathrm{dsi}}\rho_{\mathrm{si}}A_{\mathrm{si}}}{\omega}\sqrt{\frac{2\left(p_{\mathrm{si}}-p_{\mathrm{cyi}}\right)}{p_{\mathrm{si}}}} & \text{for } p_{\mathrm{cyi}}<p_{\mathrm{si}}\\ -\frac{C_{\mathrm{dsi}}\rho_{\mathrm{cyi}}A_{\mathrm{si}}}{\omega}\sqrt{\frac{2\left(p_{\mathrm{cyi}}-p_{\mathrm{si}}\right)}{\rho_{\mathrm{cyi}}}} & \text{for } p_{\mathrm{cyi}}>p_{\mathrm{si}}\end{cases} \quad (11)$$

$$\frac{\mathrm{d}m_{\mathrm{di}}}{\mathrm{d}t}=\begin{cases}\frac{C_{\mathrm{ddi}}\rho_{\mathrm{cyi}}A_{\mathrm{di}}}{\omega}\sqrt{\frac{2\left(p_{\mathrm{cyi}}-p_{\mathrm{di}}\right)}{\rho_{\mathrm{cyi}}}} & \text{for } p_{\mathrm{di}}<p_{\mathrm{cyi}}\\ -\frac{C_{\mathrm{ddi}}\rho_{\mathrm{di}}A_{\mathrm{di}}}{\omega}\sqrt{\frac{2\left(p_{\mathrm{di}}-p_{\mathrm{cyi}}\right)}{\rho_{\mathrm{di}}}} & \text{for } p_{\mathrm{di}}>p_{\mathrm{cyi}}\end{cases} \quad (12)$$

where $C_{\mathrm{dsi}}$ and $C_{\mathrm{ddi}}$ are coefficient at the valve port and the valve opening area $A_{\mathrm{si}}$ and $A_{\mathrm{di}}$ can be given as following.

$$\begin{cases}A_{\mathrm{si}}=\pi d_{\mathrm{si}}z_{\mathrm{si}}\\ A_{\mathrm{di}}=\pi d_{\mathrm{di}}z_{\mathrm{di}}\end{cases} \quad (13)$$

where $d_{\mathrm{si}}$ and $d_{\mathrm{di}}$ are the diameters of valve port. $z_{\mathrm{si}}$ and $z_{\mathrm{di}}$ represent the distance between valve plate and valve port,

respectively, and their calculating method is shown as below [18].

$$\begin{cases} M_{\mathrm{si}}\frac{d^2 z_{\mathrm{si}}}{\mathrm{d}t^2} = \beta_{\mathrm{si}} A_{\mathrm{si}}\left(p_{\mathrm{si}} - p_{\mathrm{cyi}}\right) - k_{\mathrm{si}}\left(z_{\mathrm{si}} + z_{\mathrm{s0i}}\right) \\ M_{\mathrm{di}}\frac{d^2 z_{\mathrm{di}}}{\mathrm{d}t^2} = \beta_{\mathrm{di}} A_{\mathrm{di}}\left(p_{\mathrm{cyi}} - p_{\mathrm{di}}\right) - k_{\mathrm{di}}\left(z_{\mathrm{di}} + z_{\mathrm{d0i}}\right) \end{cases} \tag{14}$$

As collision occurs between the valve plate and limiter or valve seat, an impact force is generated and the velocity relationship can be expressed as below [18].

$$\begin{cases} \left(\frac{\mathrm{d}z_{\mathrm{si}}}{\mathrm{d}t}\right)_{\mathrm{reb}} = -C_{\mathrm{rsi}}\left(\frac{\mathrm{d}z_{\mathrm{si}}}{\mathrm{d}t}\right)_{\mathrm{imp}} \\ \left(\frac{dz_{\mathrm{di}}}{\mathrm{d}t}\right)_{\mathrm{reb}} = -C_{\mathrm{rdi}}\left(\frac{\mathrm{d}z_{\mathrm{di}}}{\mathrm{d}t}\right)_{\mathrm{imp}} \end{cases} \tag{15}$$

where $C_{\mathrm{rsi}}$ and $C_{\mathrm{rdi}}$ are rebound coefficient.

## Thermodynamic process in intercoolers

The details of integrated intercoolers applicable to the miniature multi-stage reciprocating compressor are presented in Fig. 3. Three independent intercoolers and coolant channel are set in the integrated block with dimension of Φ 110 mm × 20 mm. The compressed gas from *i*th cylinder is stored and cooled in *j*th intercooler and then inhaled into $(i+1)$th cylinder. Circular channel with excellent flow capacity and machinability is chosen by referring to traditional multi-stage compressor. Screw thread is designed at the top of channel for simplified sealing of high-pressure gas with bolt and sealant, which can effectively reduce the radial and axial dimension.

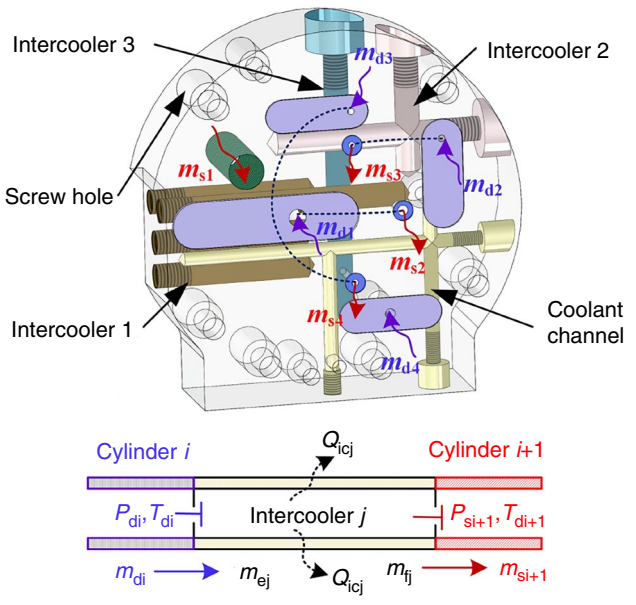


**Fig. 3** Schematic of working principle and thermodynamic process of the intercoolers

The establishment of thermodynamic model in intercoolers considering the transient heat transfer is introduced in the part.

(1) Energy and mass model.

According to the thermodynamic process interpreted in Fig. 3, energy conservation equation in the *j*th intercooler volume can be given as following.

$$\frac{\mathrm{d}Q_{\mathrm{ic\,j}}}{\mathrm{d}t} + h_{\mathrm{e\,j}}\frac{\mathrm{d}m_{\mathrm{e\,j}}}{\mathrm{d}t} = h_{\mathrm{f\,j}}\frac{\mathrm{d}m_{\mathrm{f\,j}}}{\mathrm{d}t} + m_{\mathrm{ic\,j}}\frac{\mathrm{d}h_{\mathrm{ic}j}}{\mathrm{d}t} + h_{\mathrm{ic\,j}}\frac{\mathrm{d}m_{\mathrm{ic\,j}}}{\mathrm{d}t} - V_{\mathrm{ic\,j}}\frac{dp_{\mathrm{ic\,j}}}{\mathrm{d}t} \tag{16}$$

where $\dot{Q}_{\mathrm{ic\,j}}$ represents heat transfer rate between coolant and compressed gas in the *j*th intercooler. Subscripts e and f stand for in and out.

The mass conservation equation can be given by

$$\begin{cases} \frac{\mathrm{d}m_{\mathrm{e\,j}}}{\mathrm{d}t} = \frac{\mathrm{d}m_{\mathrm{di}}}{\mathrm{d}t} \text{ for } i = j \\ \frac{\mathrm{d}m_{\mathrm{f\,j}}}{\mathrm{d}t} = \frac{\mathrm{d}m_{\mathrm{s}(i+1)}}{\mathrm{d}t} \text{ for } i = j \\ \frac{\mathrm{d}m_{\mathrm{ic\,j}}}{\mathrm{d}t} = \frac{\mathrm{d}m_{\mathrm{e\,j}}}{\mathrm{d}t} - \frac{\mathrm{d}m_{\mathrm{f\,j}}}{\mathrm{d}t} \end{cases} \tag{17}$$

2. Heat transfer model.

In Eq. (16), heat transfer item $\frac{\mathrm{d}Q_{\mathrm{ic\,j}}}{\mathrm{d}t}$ can be calculated by the following equation.

$$\frac{\mathrm{d}Q_{\mathrm{ic\,j}}}{\mathrm{d}t} = \psi_{\mathrm{ic\,j}} A_{\mathrm{ic\,j}} \Delta T_{\mathrm{ic\,j}} \tag{18}$$

where $A_{\mathrm{ic\,j}}$ is the surface area and $\Delta T_{\mathrm{ic\,j}}$ is the temperature difference between inter-stage compressed gas and the coolant, which can be expressed as below.

$$\Delta T_{\mathrm{ic\,j}} = \frac{\Delta t_{\mathrm{j\,max}} - \Delta t_{\mathrm{j\,min}}}{\ln \Delta t_{\mathrm{j\,max}} - \ln \Delta t_{\mathrm{j\,min}}} \tag{19}$$

where $\Delta t_{\mathrm{j\,max}}$ is the maximum temperature difference between compressed gas in *j*th intercooler and the coolant, while $\Delta t_{\mathrm{j\,min}}$ represents the minimum value.

Item $\psi_{\mathrm{ic\,j}}$ in Eq. (18) is the overall heat transfer coefficient and can be calculated as following.

$$\psi_{\mathrm{ic\,j}} = \frac{1}{\frac{1}{\alpha_{\mathrm{ic\,j}}} + \frac{\delta_{\mathrm{w\,j}}}{\lambda_{\mathrm{w\,j}}} + \frac{1}{\alpha_{\mathrm{co}}}} \tag{20}$$

where $\alpha_{\mathrm{ic\,j}}$ is the convection heat transfer coefficient between the compressed gas and the internal wall in *j*th intercooler and $\delta_{\mathrm{w\,j}}$ and $\lambda_{\mathrm{w\,j}}$ are the thickness and thermal conductivity of wall, respectively. $\alpha_{\mathrm{co}}$ is the convection heat transfer coefficient between intercooler and coolant. It is noteworthy that the value of $\delta_{\mathrm{w\,j}}$, $\lambda_{\mathrm{w\,j}}$ and $\alpha_{\mathrm{co}}$ can be set as fixed when

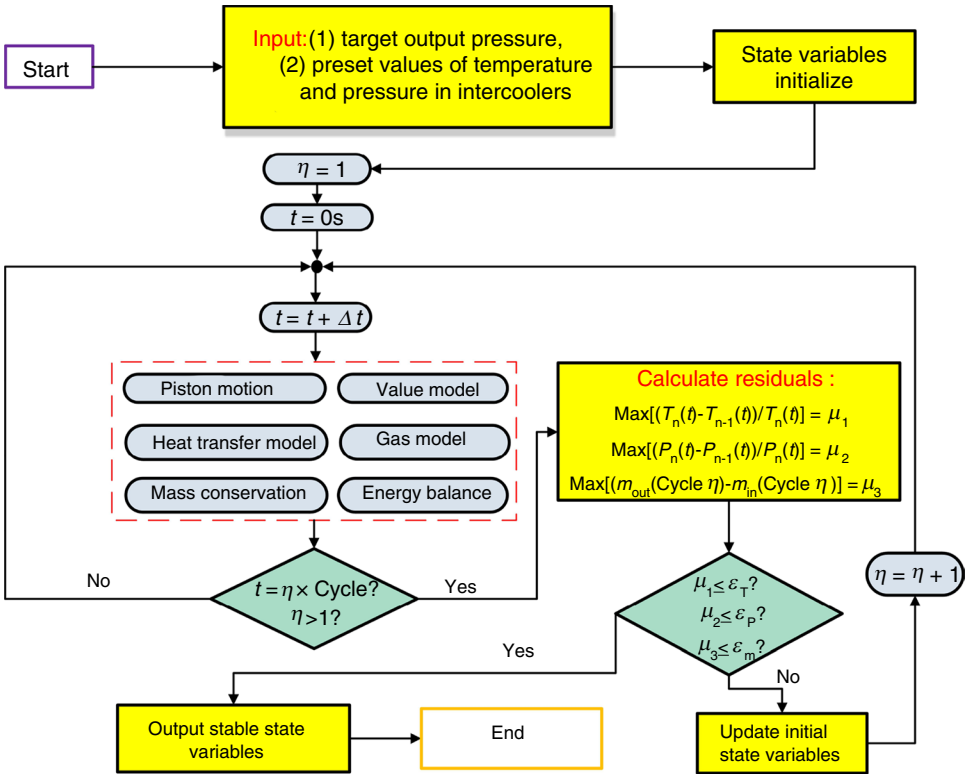


**Fig. 4** Solution flowchart of stage-in-series mathematical model

**Table 1** Intercooler parameters for numerical simulation

| Channel diameter/mm | Intercooler channel length/mm | | | Intercooler volume/mm$^3$ | | | Piston stroke volume/mm$^3$ | | | |
|---|---|---|---|---|---|---|---|---|---|---|
| | Ic1 | Ic2 | Ic3 | Ic1 | Ic2 | Ic3 | Cy1 | Cy2 | Cy3 | Cy4 |
| 4 | 225 | 95 | 78 | 2827.4 | 1193.8 | 980.2 | 19,158.7 | 4789.7 | 989.6 | 356.3 |
| 5 | | | | 4417.9 | 1865.3 | 1531.5 | | | | |
| 6 | | | | 6361.7 | 2686.1 | 2205.4 | | | | |
| 7 | | | | 8659.0 | 3656.0 | 3001.8 | | | | |

the compressor structure and coolant flow are determined. However, $\alpha_{ic\,j}$ can vary greatly with the real-time velocity, density, temperature of gas inside the intercooler, which is determined by the combined motions of the former discharge valve and the subsequent suction valve. The calculating method of $\alpha_{ic\,j}$ is introduced in the following part.

3. Determination of real-time value of heat transfer coefficient $\alpha_{ic\,j}$.

The value of $\alpha_{ic\,j}$ can be determined as following.

$$\alpha_{ic\,j} = \frac{Nu_{ic\,j}\lambda_{ic\,j}}{\tilde{D}_j} \tag{21}$$

where $\lambda_{ic\,j}$ is the thermal conductivity of gas and $\tilde{D}_j$ is the hydraulic diameter of the flow channel. $Nu_{ic\,j}$ is Nusselt number, and it can be calculated as below.

When the former discharge valve and the subsequent suction valve are both closed, natural convection heat transfer is applied to the calculation of $Nu_{ic\,j}$ as below.

$$Nu_{ic\,j} = \begin{cases} 0.197\left(Gr_j Pr_{f\,j}\right)^{1/4}\left(\frac{l_j}{\delta_j}\right)^{-1/9} & \text{if } 8.6\times10^3 \le Gr_j \le 2.9\times10^5 \\ 0.073\left(Gr_j Pr_{f\,j}\right)^{1/3}\left(\frac{l_j}{\delta_j}\right)^{-1/9} & \text{if } 2.9\times10^5 \le Gr_j \le 1.6\times10^7 \end{cases} \tag{22}$$

where $Gr_j$ is the Grashof number and $Pr_{f\,j}$ is Prandtl number. $l_j$ is the length of flow channel, and $\delta_j$ is the wall thickness.

Grashof number can be given as below.

$$Gr_j = \frac{g\varepsilon_{vj}\left(t_{hj} - t_{lj}\right)\delta_j^3}{\left(\frac{\eta_j}{\rho_j}\right)^2} \tag{23}$$

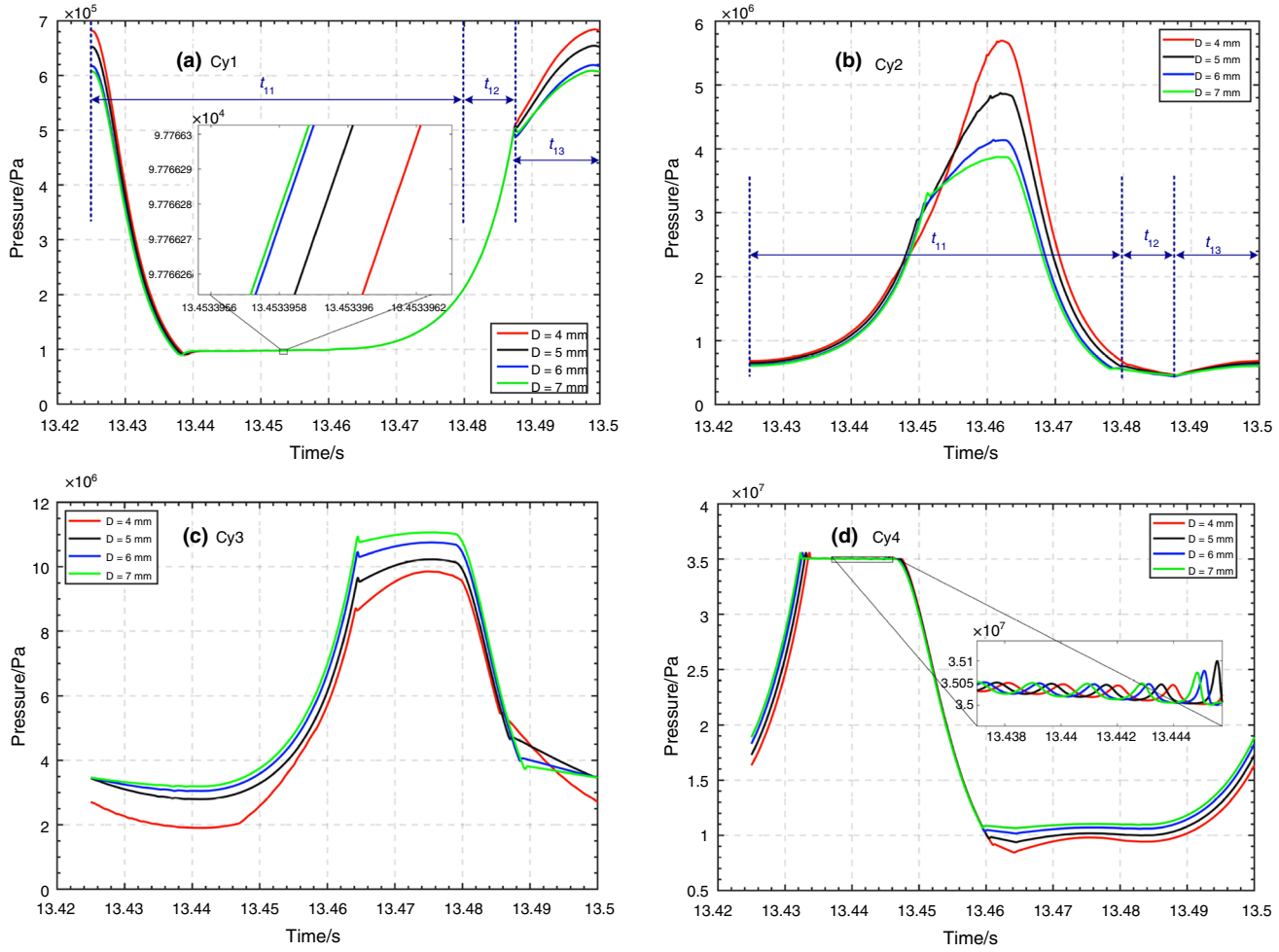


**Fig. 5** Gas pressure in each cylinder

where $\varepsilon_{vj}$, g and $\eta_j$ stand for volume expansion coefficient, gravitational constant and dynamic viscosity, respectively.

When the former discharge valve or the subsequent suction valve is open, forced convection heat transfer is applied to the calculation of $Nu_{ic\,j}$.

$$Nu_{ic\,j}=\begin{cases}1.86\left(\dfrac{\eta_{f\,j}}{\eta_{w\,j}}\right)^{0.14}\left(\dfrac{Re_j Pr_{f\,j}}{l_j/\tilde{D}_j}\right) & \text{laminer flow}\\ \dfrac{(f_j/8)(Re_j-1000)Pr_{f\,j}}{1+1.27\sqrt{f_j/8}(Pr_{f\,j}^{2/3}-1)}\left(\dfrac{T_{f\,j}}{T_{w\,j}}\right)^{0.01}\left[1+\left(\dfrac{\tilde{D}_j}{l_j}\right)^{2/3}\right] & \text{turbulance flow}\end{cases} \tag{24}$$

where $T_{f\,j}$ and $T_{w\,j}$ are average temperature of compressed gas and wall surface and $\eta_{f\,j}$ and $\eta_{w\,j}$ are the corresponding dynamic viscosity of compressed gas under the temperature of $T_{f\,j}$ and $T_{w\,j}$, respectively.

In Eq. (24), the Reynolds number $Re_j$ and Darcy resistance coefficient $f_j$ can be determined as following, respectively.

$$Re_j=\frac{\tilde{D}_j}{S_j\eta_{f\,j}}\frac{dm_{ic\,j}}{dt} \tag{25}$$

$$f_j=(1.82\lg Re_j-1.64)^{-2} \tag{26}$$

where $S_j$ is the cross-sectional area of the channel.

## Numerical implementation

Matlab/Simulink was used to implement the stage-in-series thermodynamic models. The mathematic models of former cylinder and subsequent cylinder were connected by intercooler model, as interpreted in Fig. 2. Structural parameters of cylinders and intercoolers were present in the model, as well as the initial pressure and temperature. Fixed-step fourth-order Runge–Kutta (ode45) algorithm was adopted for solution, and the solution flowchart is shown in Fig. 4. Two convergence criterions were set to guarantee the stable state which had been reached. Firstly, the maximum pressure difference and temperature difference between two iterations in each control body at the same shaft position were less than the set residual error. Secondly, the gas mass difference

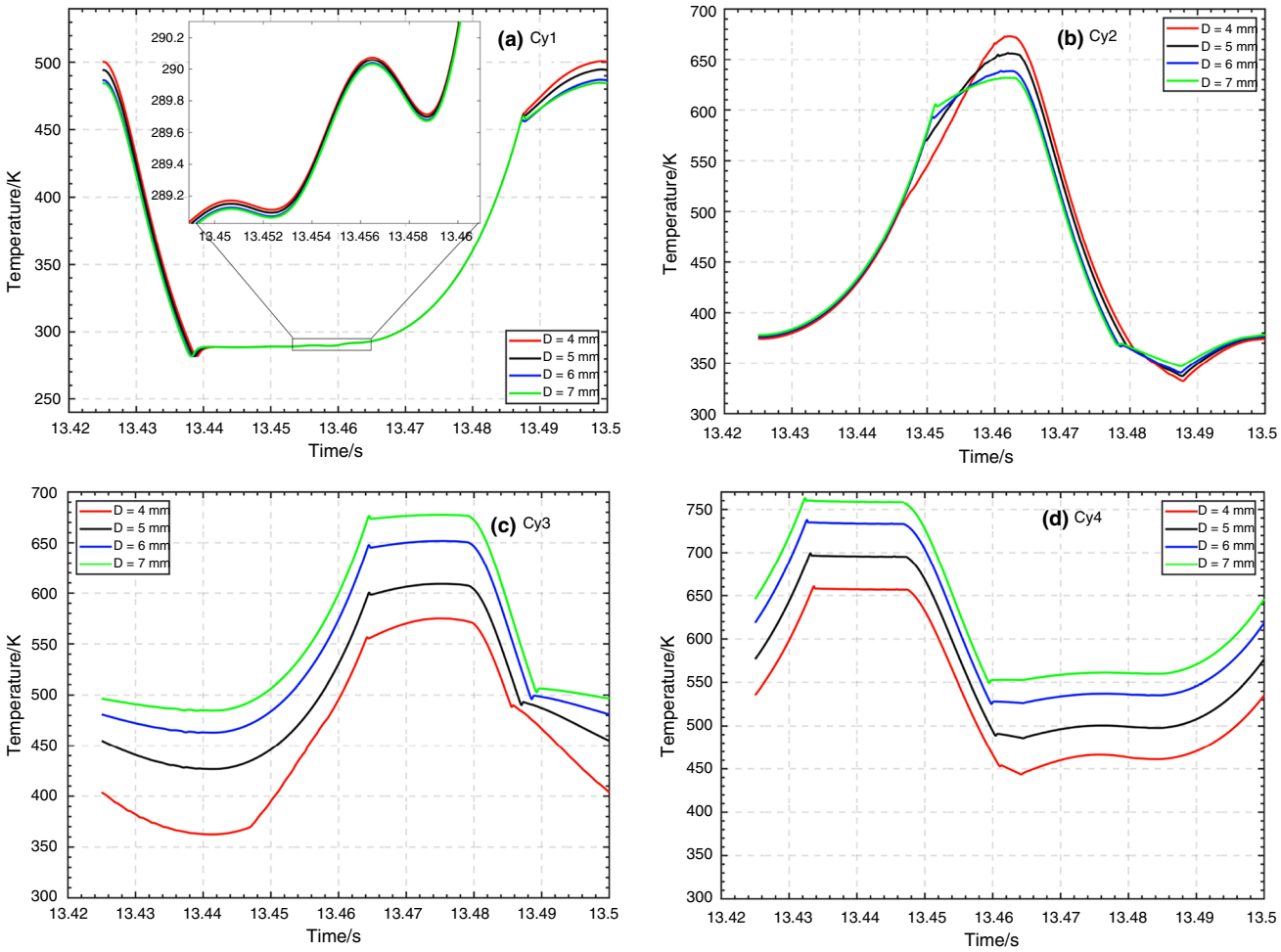


**Fig. 6** Gas temperature in each cylinder

between the outflow and inflow of each control volume was less than the set residual error.

## Numerical results and discussion

According to the structure of integrated intercooler presented in Fig. 3, we set the values of channel length as fixed while varying the channel diameter. The maximum channel diameter can reach to 7 mm under current overall dimension setting. Table 1 presents the comparison of intercooler volume (Ic) and cylinder volume (Cy). It can be learned that the values of Ic1 are obviously smaller than Cy2 when the channel diameter is 3 mm, while Ic 2 is equivalent to Cy3. When the diameter increases to 7 mm, the volume of Ic1 is still 1.8 times that of Cy1. The intercooler volumes are obviously insufficient in the miniature multi-stage compressor compared to traditional design criterion, especially for Cy2 and Cy3.

### In-cylinder thermodynamic properties

For quantitative assessment of the effects of the inter-stage volumes, the discharge pressure was set fixed as 35 MPa and a stable period as interpreted in Fig. 4 was selected. Based on the parameters listed in Table 1, the variations of in-cylinder gas pressure and gas temperature with different intercooler channel diameters are presented in Fig. 5 ad Fig. 6, respectively. It can be learned that the inter-stage volume exerts great influence on discharge pressure in Cy1 and Cy2. The pressure peak in Cy1 and Cy2 reaches to 0.68 MPa and 5.71 MPa, respectively, when the diameter is 4 mm. As the channel diameter increases to 7 mm, the pressure peak drops to 0.61 MPa and 3.82 MPa, respectively. As for Cy 3, the suction pressure and discharge pressure increase with the channel diameter, which results in the increasing suction pressure in Cy4. The diameters of first stage piston and second stage piston are relatively large, and it can be inferred that increasing the inter-stage volume of Ic1 and

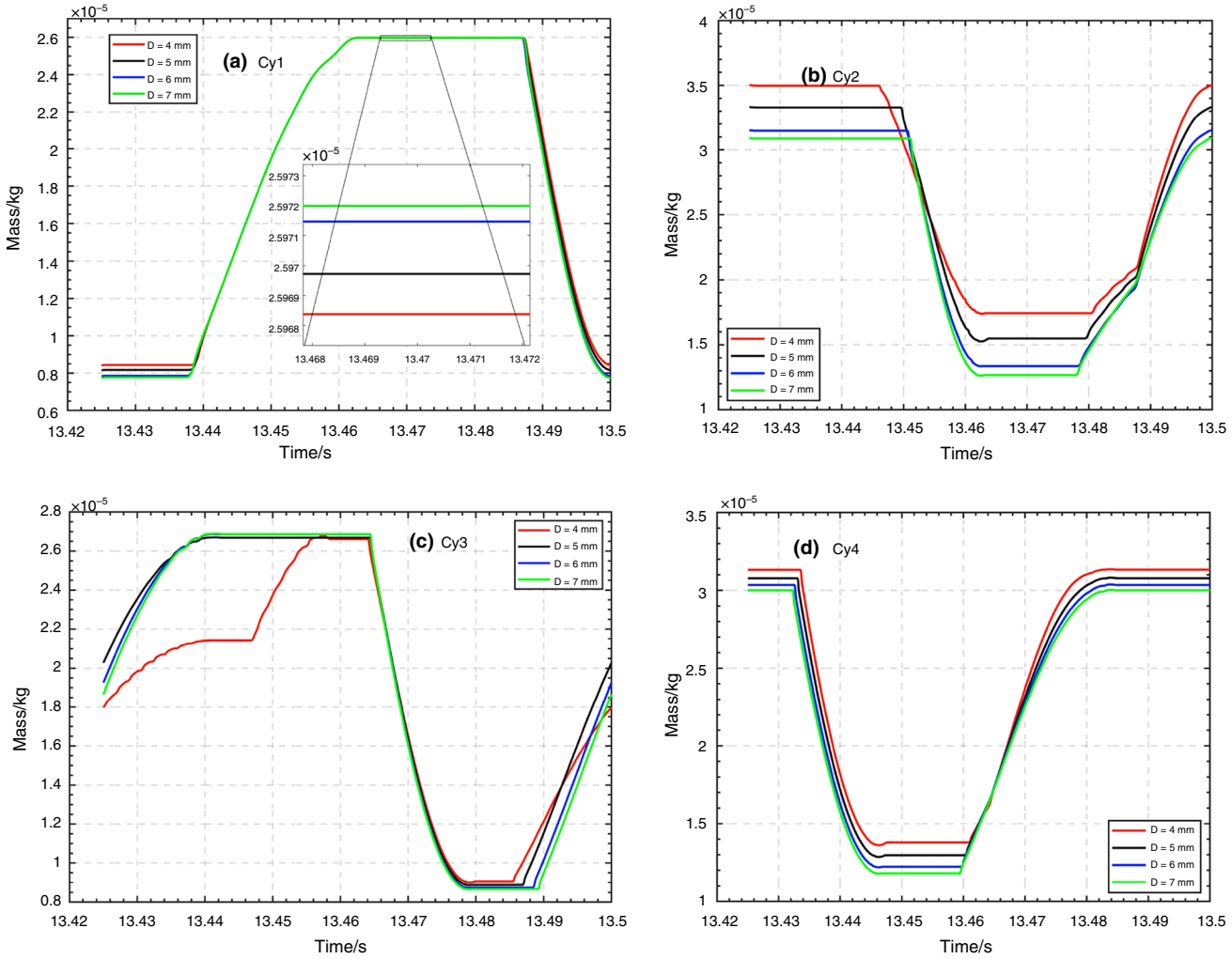


**Fig. 7** Gas mass in each cylinder

Ic2 can reduce the pressure peak in Cy1 and Cy2, which is beneficial for reduction of frictional power loss.

As for gas temperature in Fig. 6, we can learn that its variation in Cy1, Cy2 and Cy3 follows the variation trends of gas pressure. In Cy4, gas temperature at the discharge process varies greatly with the channel diameter when the discharge pressure is set fixed. Additionally, it can be observed that the average temperature Cy4 is significantly higher than Cy1, which can attribute to the insufficient cooling with limited volumes. More severe wear of piston sealing parts can occur under such temperature range.

Figure 7 illustrates the variations of gas mass in each cylinder during one cycle. The gas mass during the expansion process in Cy1, Cy2 and Cy3 is smaller when the diameter is larger due to the relative lower discharge pressure. In Cy4, higher discharge temperature can result in less mass during the expansion process. Additionally, it can be noticed in Fig. 7c that gas mass during the suction and compression process shows a different variation trend when the diameter is 4 mm. The gas mass keeps fixed at a medium value for a period and then continues to rise to the maximum value, which indicates the suction valve of Cy3 experiences abnormal opening and closing movement at the corresponding process.

## Valve dynamics

The movement of suction valves and discharge valves varied with inter-stage volume is presented in Figs. 8 and 9. The opening time of suction valves in Cy1, Cy2 and Cy4 delays with the decrease in channel diameter. It is because that the discharge pressures in Cy1 and Cy2 increase when channel diameter decreases, the expansion process will take longer time to reach the opening differential pressure of suction valve. As for Cy4, gas mass is less in the cylinder at the end of discharge process when channel diameter is smaller,

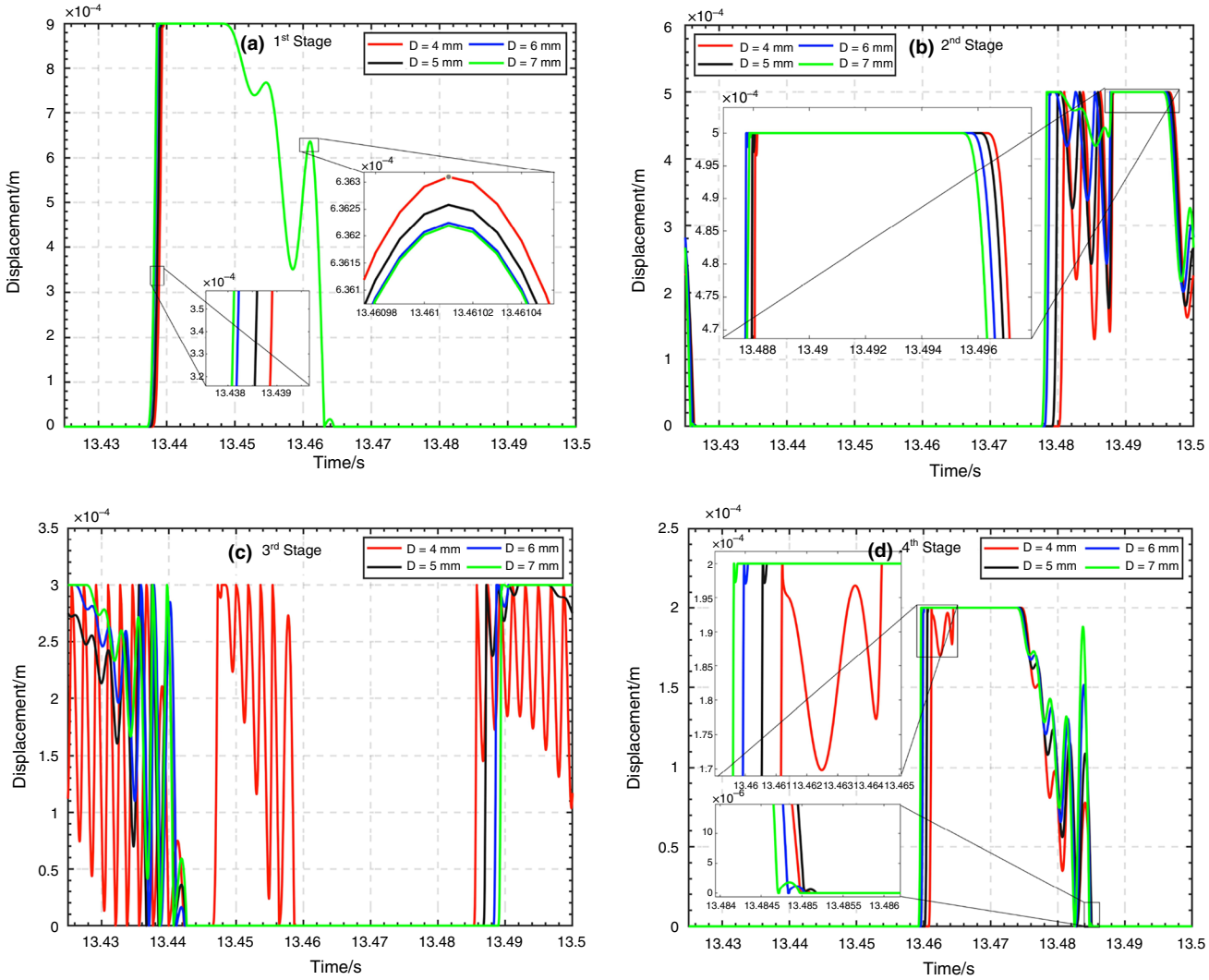


**Fig. 8** Displacement of suction valves

the pressure can fall faster to reach the opening differential pressure. This can also explain the opposite phenomenon of Cy3 presented in Fig. 8c. It is noteworthy that the suction valve in Cy3 experiences repeated opening when the channel diameter is 4 mm, which results in the intermittent rise of air mass as shown in Fig. 7c. Violent oscillation occurs when the suction valve plate of Cy2 and Cy3 collides with the lift limiter and the oscillation amplitude increases as the channel diameter decreases. All suction valves experience violent oscillation when the valve plates leave the lift limiter.

It can be learned from Fig. 9 that the full-open time of all discharge valves are inadequate under insufficient inter-stage volumes. The discharge valves of first stage and third stage maintain full-open status for a short time when the channel diameter is 7 mm. However, when the diameter decreases to 4 mm, the valve plate rebounds after collision with lift limiter and then quickly falls back to the valve seat. As for the second stage discharge valve, the valve plate experiences multiple collisions with the lift limiter when the diameter is less than 7 mm. It can attribute to the greater pressure fluctuations in intercoolers with more insufficient inter-stage volumes, which will be discussed in the following section.

To sum up, insufficient inter-stage volumes contribute to abnormal movement of suction and discharge valves in miniature multi-stage reciprocating compressor. The abnormal movement is more obvious when the volumes are less and the service life and reliability of compressors can be greatly weakened.

## In-intercooler thermodynamic properties

The variations of in-intercooler gas pressure, temperature, mass and transient heat transfer coefficient with different intercooler channel diameters are discussed in this section.

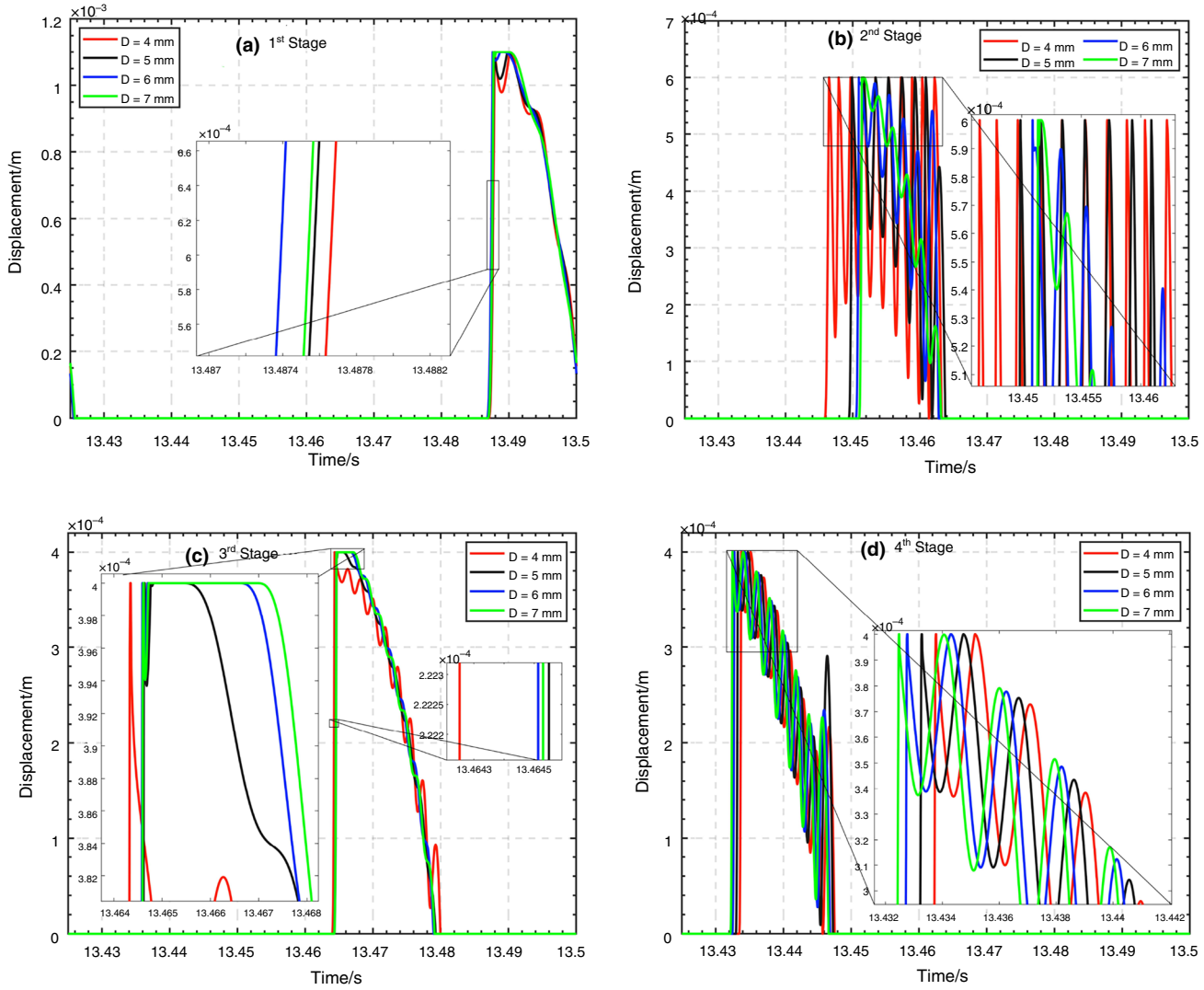


**Fig. 9** Displacement of discharge valves

Figure 10 shows the thermodynamic properties of Ic1 in five cycles. During the period of $t_{11}$, Cy1 is in the expansion and suction process while Cy2 is in the compression and discharge process, which mean the discharge valve of Cy1 and suction valve of Cy2 are both closed and natural convection heat transfer is formed inside Ic1. Subsequently, Cy1 experiences compression process while Cy2 experiences suction process during the $t_{12}$ period. The suction valve of Cy2 is opened, forced convection is formed, and the transient heat transfer coefficient increases rapidly. Moreover, when time advances to $t_{13}$, both the discharge valve of Cy1 and suction valve of Cy2 are opened, and forced convection heat transfer is further strengthened.

It can also be learned that the gas pressure peak in Ic1 increases with the decrease in channel diameter at the same time, while the curves of temperature and mass show opposite variation trends. The fluctuation amplitude of temperature and pressure are obviously larger when the channel diameter decreases, which can bring about more serious vibration, frictional loss and power consumption. Additionally, the transient heat transfer coefficient distinguishes significantly with the channel diameter. Smaller diameter can bring about faster flow velocity in the channel, and the Reynolds number increases greatly and thus enhances the heat transfer.

The variations of thermodynamic properties in Ic2 are shown in Fig. 11. Pressure and temperature fluctuation are more evident with variation of channel diameter. The maximum and minimum pressure differences are 3.81 MPa and 0.65 MPa when the diameters are 7 mm and 4 mm,

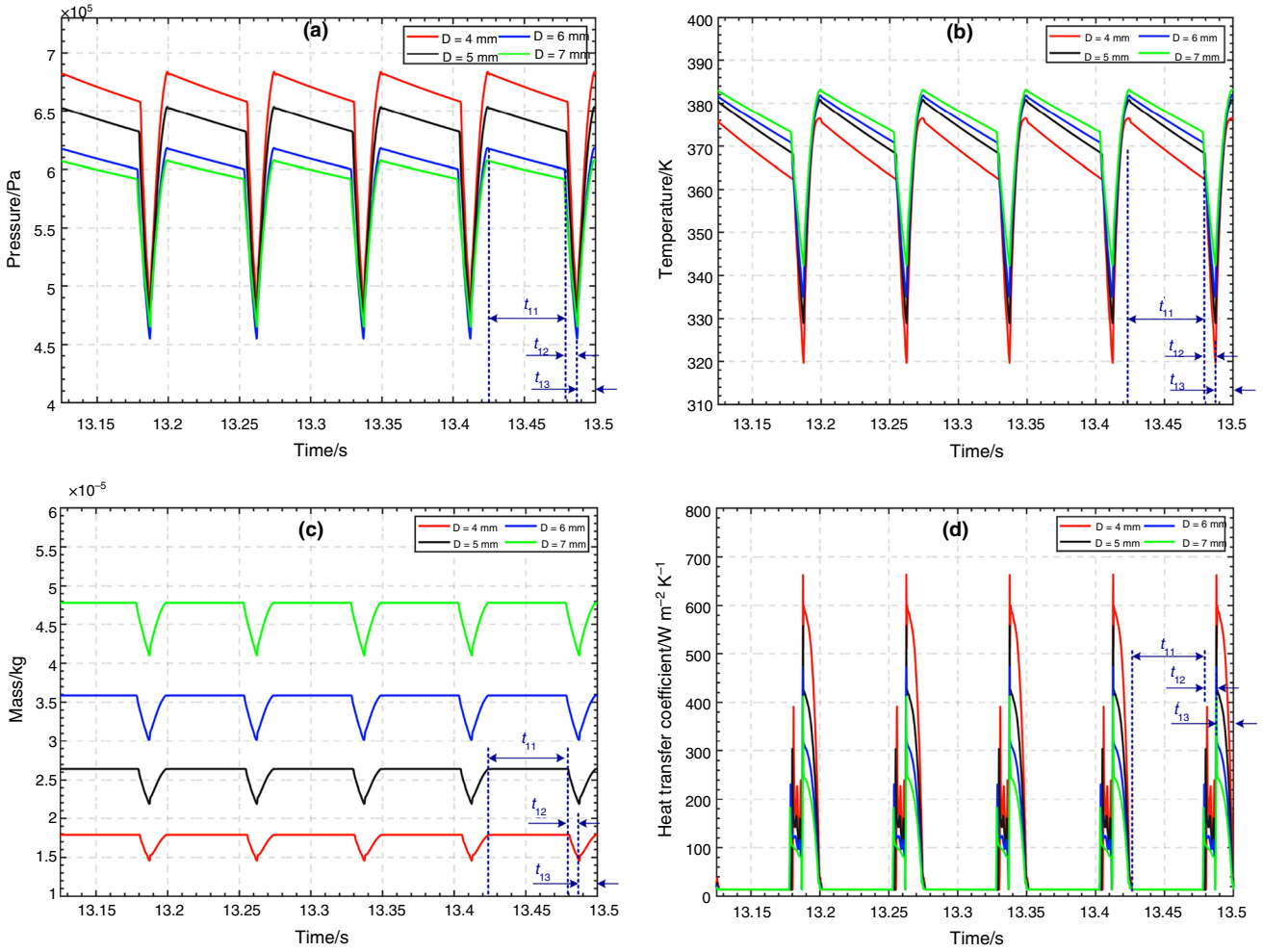


**Fig. 10** Variations of thermodynamic properties in Ic1

respectively. Higher pressure in Ic2 will exert significant effects on the pressure in Cy2 and lead to more frictional loss due to the relative large diameter of 2nd piston.

Figure 12 shows the variations of thermodynamic properties in Ic3. It can be learned that pressure and temperature fluctuation reduce to a certain extent compared to Ic2. The maximum and minimum pressure differences are 1.38 MPa and 0.40 MPa when the diameters are 7 mm and 4 mm, respectively. Compared to former two intercoolers, the pressure inside Ic3 increases with the channel diameter, which can somewhat result in the increment of driving force in Cy3 and Cy4. However, the diameter of third and fourth piston is small ($\leq$10 mm) and the overall power consumption is less sensitive to the variation of gas pressure.

Based on the transient heat transfer coefficient described in the above three figures, the total heat flow of the intercoolers in one cycle has been calculated and is presented in Fig. 13. It can be learned that the variation of heat flow is more distinctive when channel diameter is 4 mm. The abnormal opening and closing movement of suction valve and discharge valve under such inter-stage cooling brings about the multiple occurrences of heat flow peaks.

## Flow rate and indicated work

The overall thermodynamic performance of the miniature multi-stage reciprocating compressor with different inter-stage volumes has been presented in this section. Figure 14 shows the variations of *p*–*V* diagram of each cylinder. Based on Fig. 14, the indicated work is calculated and presented in Fig. 15. The indicated work of Cy1 decreases with the channel diameter, while the other three cylinders show opposite trend. The discharge pressure of Cy1 is obviously higher when the channel diameter is smaller, resulting in more indicated work in the cylinder. It is noteworthy that although the relative variations of indicated work under

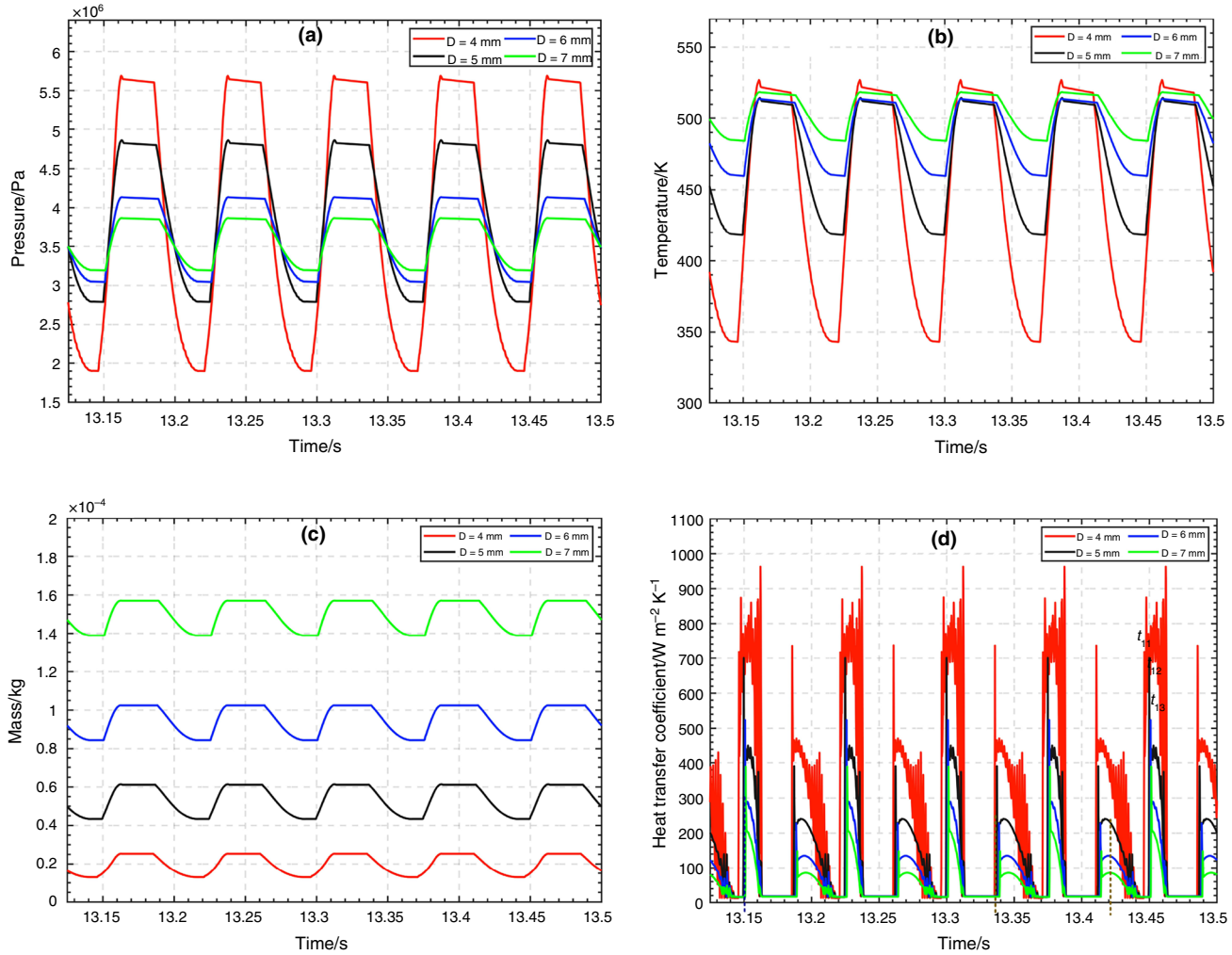


**Fig. 11** Variations of thermodynamic properties in Ic2

different inter-stage volumes are quite small, the frictional loss caused by the increasing in-cylinder pressure in Cy1 and Cy2 is significant due to the large piston diameters.

The volumetric flow rate and total indicated work of the miniature multi-stage compressor are presented in Fig. 16. The flow rate increases from 10.84 SL $min^{-1}$ to 11.26 SL $min^{-1}$ when channel diameter increases from 4 to 7 mm. The total indicated work also increases with the channel diameter. It can be inferred that enhancing the inter-stage cooling can improve the volumetric efficiency to a certain extent, as presented in Fig. 17. The overall volumetric efficiency of the compressor increases from 70.82% to 73.56% when channel diameter increases from 4 to 7 mm.

## Experimental investigation

Experimental test rig has been established to validate the mathematical model and further investigate the overall performance of the compressor with different intercooler volumes. As shown in Fig. 18, the compressor was driven by a brushless motor to run at a speed of 800 r/min. A gas receiver with volume of 0.7 L was used to store the high-pressure gas. The pressure and temperature in the gas receiver were recorded to calculate the average flow rate of the compressor. The input current of brushless motor was monitored and recorded simultaneously. The test was started when pressure in gas receiver reached 25 MPa, and the data were recorded for every one minute. Intercoolers with channel diameters of 4 mm and 7 mm were used for comparison, as shown in Fig. 19. As interpreted in Fig. 3 and Table 1, the gas channels with diameter of 4 mm and 7 mm were sealed by M5 and M10 screws, respectively.

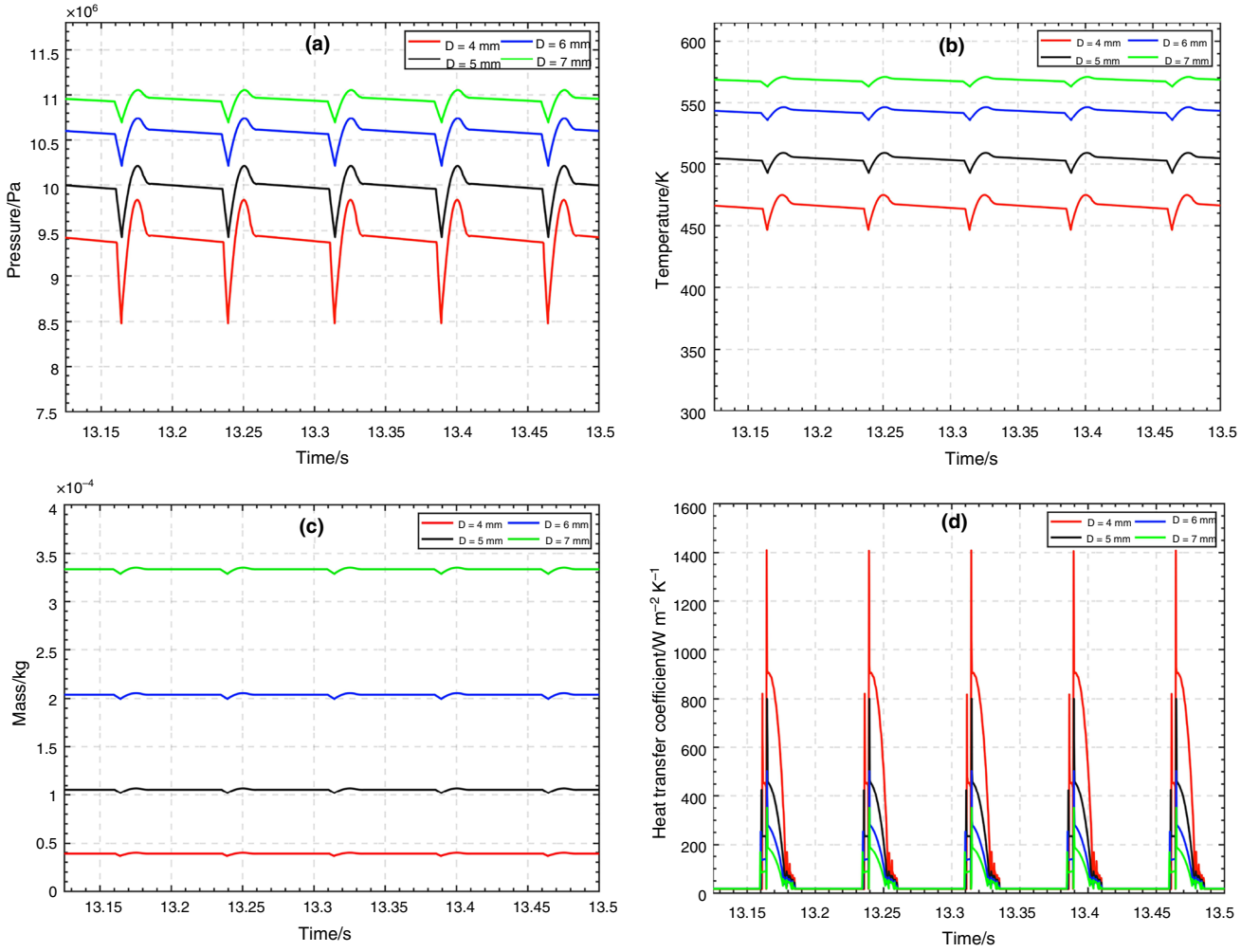


**Fig. 12** Variations of thermodynamic properties in Ic3

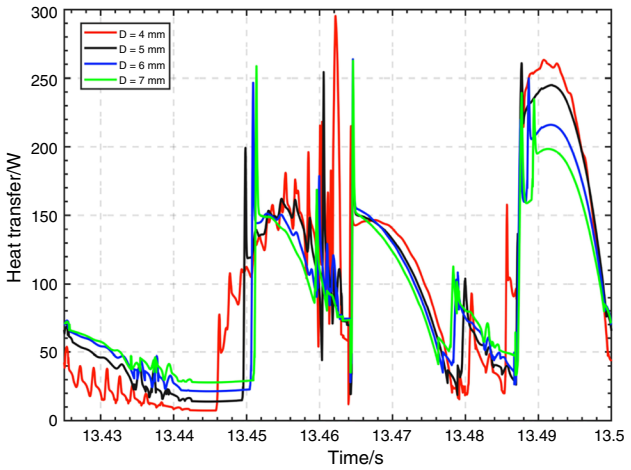


**Fig. 13** Total heat flow inside the intercoolers (one cycle)

Figure 20 compares the experimental output pressure and motor current with pressurization time. It can be learned that the pressure is basically linear with time, which indicates that the flow rate is uniform along with the discharge pressure. Additionally, the pressure rising process is slightly slower when the channel diameter is 4 mm. It is noteworthy that the variation trends of motor current show significant difference compared to output pressure. Motor current is 1.95 A and 2.33 A with output pressure of 25 MPa when the channel diameter is 7 mm and 4 mm, respectively. After 6 min operating time, the motor current increases to 2.18 A and 2.78 A, respectively. It is evident that more insufficient inter-stage volume can result in more power consumption due to the abnormally high-pressure gas inside the former-stage cylinders. Therefore, it is essential to enlarge the inter-stage volume between the low-pressure cylinders.

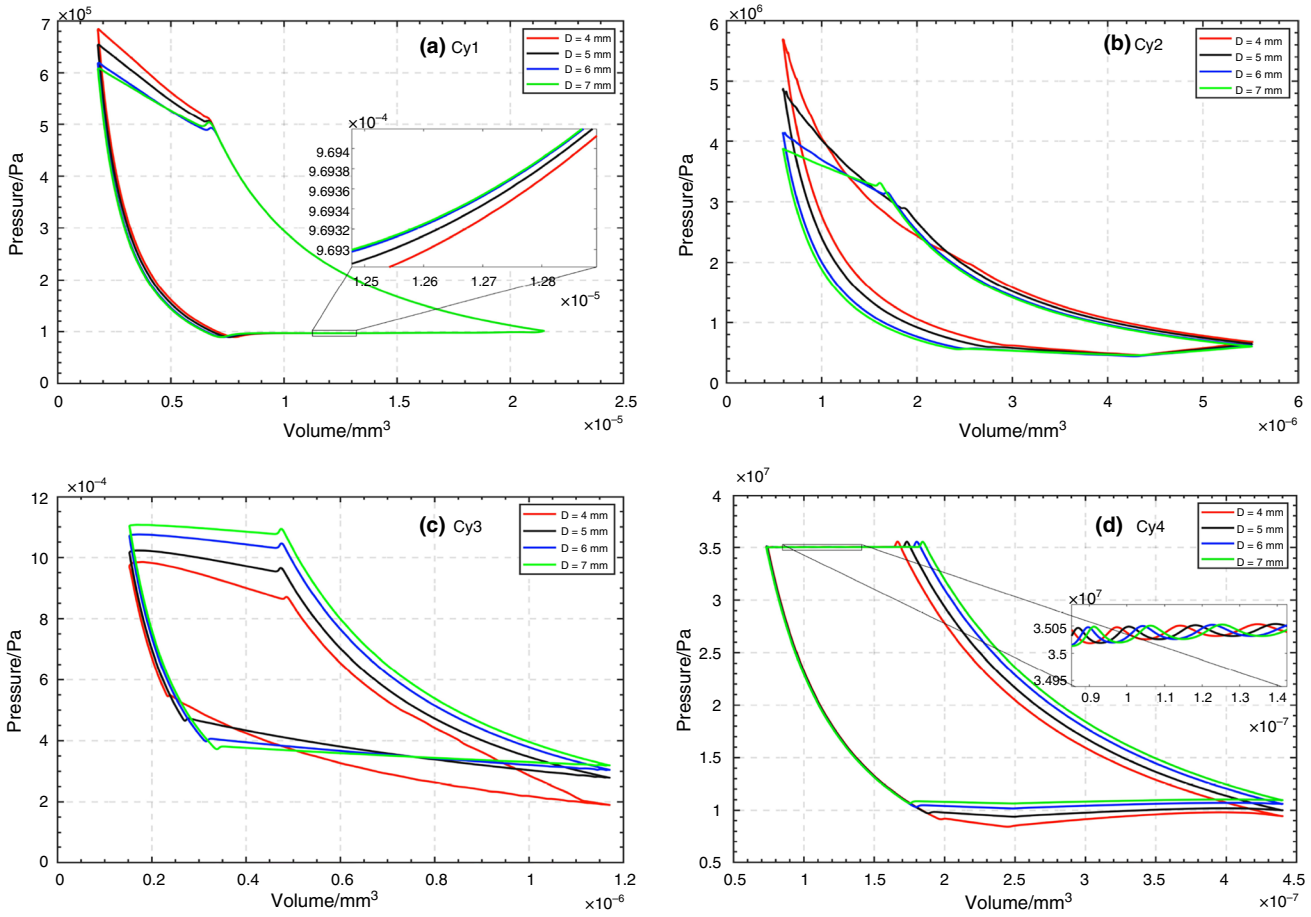


**Fig. 14** Variations of *p*–*V* diagram of each cylinder

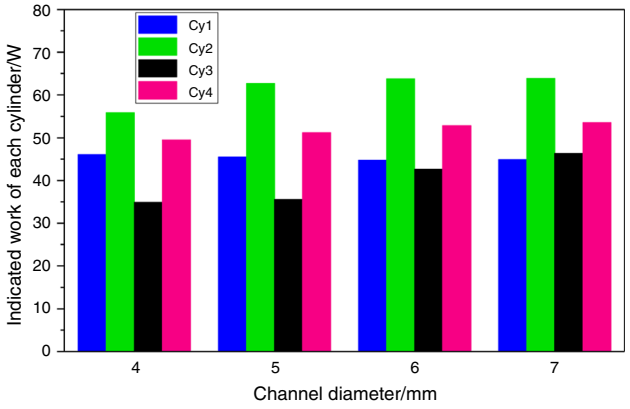


**Fig. 15** Comparison of indicated work in each cylinder

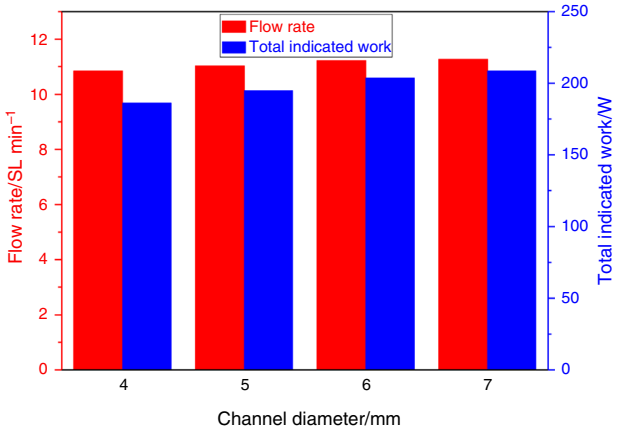


**Fig. 16** Comparison of flow rate and total indicated work

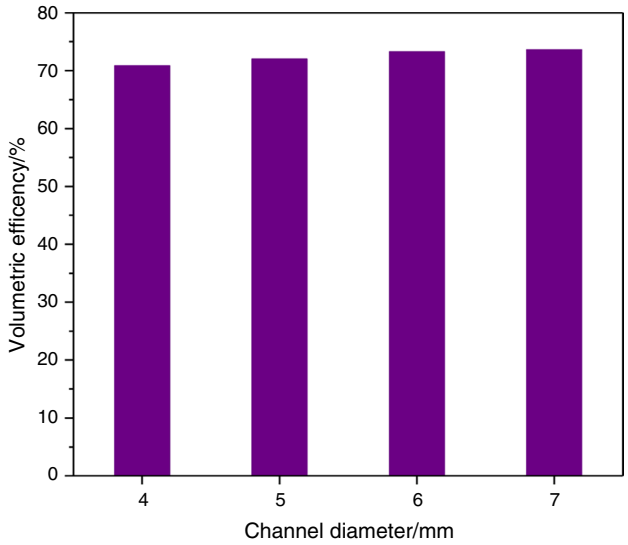


**Fig. 17** Comparison of overall volumetric efficiency

Based on the output pressure in Fig. 20, the comparison of experimental and predicted flow rate is presented in Table 2. It can be learned that the experimental flow rates are slightly lower than the predicted one. The deviations are 6.4% and 5.4% when the channel diameters are 4 mm and 7 mm, respectively. It is mainly due to that trace amounts of gas leakage occur between PTFE sealing part and pistons under high pressure. To sum up, the deviations are acceptable for engineering applications and model verification in current research.

**Fig. 18** Test rig of the miniature multi-stage compressor

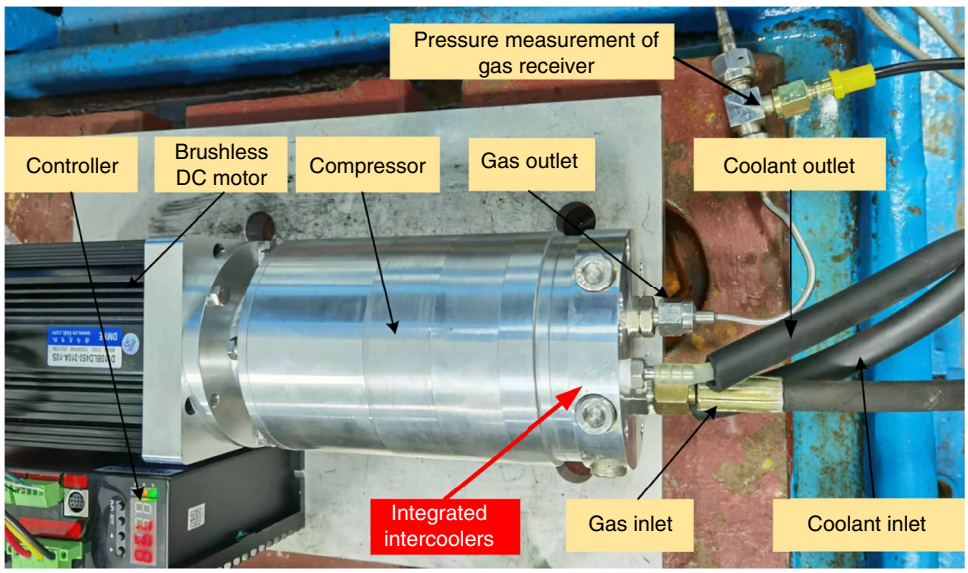


**Fig. 19** Physical drawing of the intercooler with different channel diameters

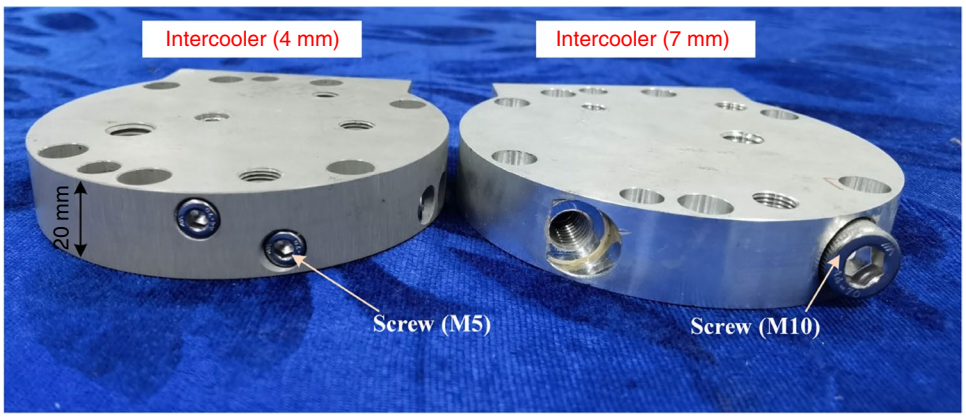

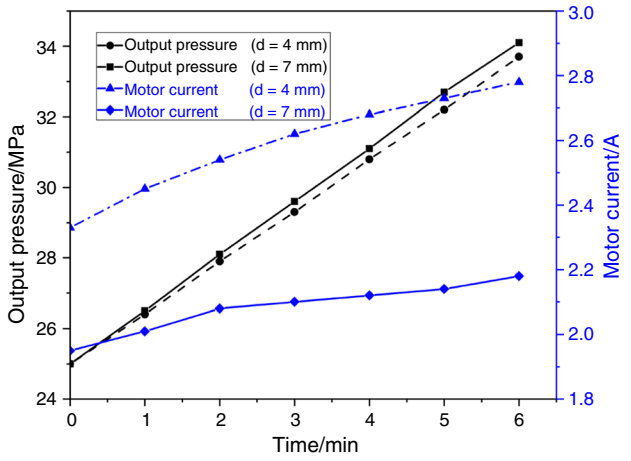


**Fig. 20** Experimental values of output pressure and motor current with pressurization time

**Table 2** Predicted and experimental flow rates of the compressor

| Diameter/mm | Predicted flow rate/SL $min^{-1}$ | Experimental flow rate/SL $min^{-1}$ | Error/% |
|---|---|---|---|
| 4 | 10.84 | 10.15 | 6.4 |
| 7 | 11.21 | 10.61 | 5.4 |

## Conclusions

This paper presents a stage-in-series mathematical model to investigate the thermodynamic performance of miniature multi-stage reciprocating compressor with insufficient inter-stage volumes. Transient heat transfer inside the intercoolers was emphasized. Different from previous work focused on in-cylinder process, the in-intercooler thermodynamic properties have been analyzed simultaneously in current work, the overall thermodynamic performance of multi-stage reciprocating compressor can be evaluated in a more accurate way. Furthermore, experimental investigation on overall performance of miniature multi-stage reciprocating compressor has been carried out. The main conclusions of current research can be made as following.

1. Inter-stage volume exerts great influence on discharge pressure and temperature of former-stage cylinders. The pressure peak in Cy1 and Cy2 increases with the decrease in channel diameter. The pressure peak increment in Cy2 is 1.89 MPa when channel diameter decreases from 7 to 4 mm.
2. Insufficient inter-stage volumes contribute to abnormal movement of suction and discharge valves in miniature multi-stage reciprocating compressor. The reliability of compressors can be greatly affected.
3. The indicated work and flow rate are slightly influenced by the channel diameter. The flow rate increases from 10.84 to 11.26 L $min^{-1}$ when channel diameter increases from 4 to 7 mm.
4. Experimental results show that the overall power consumption is sensitive to insufficient inter-stage volumes and its value increases significantly with the decrease in channel diameter.

**Acknowledgements** This research was supported by National Natural Science Foundation of China (No. 52105056).

**Authors' contribution** YD contributed to conceptualization, methodology, investigation, and writing original draft. XJ contributed to data analysis. CW and LB contributed to experiment rig. YL contributed to review and editing and supervision. KH contributed to parts manufacturer.

## Declarations

**Conflict of interest** The authors declare that they have no known competing financial interests or personal relationships that could have appeared to influence the work reported in this paper.

## References

1. Zhao B, Zhou S, Jia X, Wang M, Ma Z. Investigation of interaction between thermodynamic processes and pressure pulsation based on transient CFD model of a reciprocating compressor. Proc Inst Mech Eng Part E: J Process Mech Eng. 2021;235:1396–407.
2. Wang S, Sun J, Cao F. Investigation of flow behaviour and heat rejection for an air-cooled small multi-stage swash-plate compressor. Appl Therm Eng. 2021;192:116951.
3. Hanlon PC. Compressor handbook. New York: McGraw-Hill; 2001.
4. Bloch HP. A practical guide to compressor technology. New York: Wiley; 2006.
5. Elhaj M, Gu F, Ball AD, Albarbar A, Al-Qattan M, Naid A. Numerical simulation and experimental study of a two-stage reciprocating compressor for condition monitoring. Mech Syst Signal Process. 2008;22:374–89.
6. Wang S, Sun J, Cao F. Investigating fatigue failure of core motion mechanism for a small oil-free wobble-plate compressor. Int J Refrig. 2020;117:346–57.
7. Navarro E, Granryd E, Urchueguía JF, Corberán JM. A phenomenological model for analyzing reciprocating compressors. Int J Refrig. 2007;30:1254–65.
8. Yang B, Bradshaw CR, Groll EA. Modeling of a semi-hermetic CO2 reciprocating compressor including lubrication submodels for piston rings and bearings. Int J Refrig. 2013;36:1925–37.
9. Farzaneh-Gord M, Niazmand A, Deymi-Dashtebayaz M, Rahbari HR. Effects of natural gas compositions on CNG (compressed natural gas) reciprocating compressors performance. Energy, Part. 2015;1(90):1152–62.
10. Farzaneh-Gord M, Niazmand A, Deymi-Dashtebayaz M, Rahbari HR. Thermodynamic analysis of natural gas reciprocating compressors based on real and ideal gas models. Int J Refrig. 2015;56:186–97.

11. Roskosch D, Venzik V, Atakan B. Thermodynamic model for reciprocating compressors with the focus on fluid dependent efficiencies. Int J Refrig. 2017;84:104–16.
12. Bell IH, Ziviani D, Lemort V, Bradshaw CR, Mathison M, Horton WT, Braun JE, Groll EA. PDSim: A general quasi-steady modeling approach for positive displacement compressors and expanders. Int J Refrig. 2020;110:310–22.
13. Wang T, Wang J, Guo Y, Peng X, Yang J, Zhang Z. The study on mass transport process in the cylinder of CO2 compressor based on p–V diagram. Appl Therm Eng. 2020;174: 115314.
14. Bacak A, Pınarbaşı A, Dalkılıç AS. A 3-D FSI simulation for the performance prediction and valve dynamic analysis of a hermetic reciprocating compressor. Int J Refrig. 2023;150:135–48.
15. Zhao B, Jia X, Sun S, Wen J, Peng X. FSI model of valve motion and pressure pulsation for investigating thermodynamic process and internal flow inside a reciprocating compressor. Appl Therm Eng. 2018;131:998–1007.
16. Wu W, Guo T, Peng C, Li X, Li X, Zhang Z, Xu L, He Z. FSI simulation of the suction valve on the piston for reciprocating compressors. Int J Refrig. 2022;137:14–21.
17. Jiang X, Liu Y, Deng Y, Wang Z, Xu R. Numerical analysis of a miniature multi-stage compressor at variable altitudes based on stages-in-series method. Appl Therm Eng. 2023;219: 119563.
18. Liu Y, Miao N, Deng Y, Wu D. Efficiency evaluation of a miniature multi-stage compressor under insufficient inter-stage cooling conditions. Int J Refrig. 2019;97:169–79.
19. Deng Y, Jiang X, Pang H, Liu Y, Wang P, Liu Y. Investigation on the thermodynamic performance of a small multi-stage swash-plate compressor under different ambient temperature. Int J Refrig. 2023;145:196–207.
20. Taleb AI, Barfuß C, Sapin P, White AJ, Fabris D, Markides CN. Simulation of thermally induced thermodynamic losses in reciprocating compressors and expanders: Influence of real-gas effects. Appl Therm Eng. 2022;217:118738.
21. Rutczyk B, Szczygieł I. Development of internal heat transfer correlations for the cylinders of reciprocating machines. Energy. 2021;230:120795.
22. Liu Z, Cao X, Wang T, Jia W, Duan Z. Comparative evaluation of the refrigeration compressor performance under different valve parameters in a trans-critical CO2 cycle. Int J Refrig. 2019;101:34–46.
23. Niazmand A, Farzaneh-Gord M, Deymi-Dashtebayaz M. Exergy analysis and entropy generation of a reciprocating compressor applied in CNG stations carried out on the basis models of ideal and real gas. Appl Therm Eng. 2017;124:1279–91.